

Production cross sections and angular distributions of neutron-rich rare isotopes from 15 MeV/nucleon Kr-induced collisions: toward the r-process path

O. Fasoula^a, G.A. Souliotis^{a,*}, Y.K. Kwon^b, K. Tshoo^b
M. Veselsky^c, S.J. Yennello^d and A. Bonasera^{d,e}

^a *Laboratory of Physical Chemistry, Department of Chemistry, National and Kapodistrian University of Athens, Athens, Greece*

^b *The Rare Isotope Science Project (RISP), Institute for Basic Science, Daejeon, Korea*

^c *Institute of Experimental and Applied Physics, Czech Technical University, Prague, Czech Republic*

^d *Cyclotron Institute, Texas A&M University, College Station, Texas, USA*

^e *Laboratori Nazionali del Sud, INFN, Catania, Italy*

* *Corresponding author. Email: soulioti@chem.uoa.gr*

Abstract

We present our recent study of cross sections and angular distributions of projectile fragments from heavy-ion reactions at beam energy of 15 MeV/nucleon. We studied the production cross sections and the angular distributions of neutron-rich nuclides from collisions of a ^{86}Kr (15 MeV/nucleon) beam with heavy targets (^{64}Ni , ^{124}Sn and ^{238}U). Experimental data from our previous work at Texas A & M were compared with model calculations. Our calculations were based on a two-step approach: the dynamical stage of the collision was described with, first, the phenomenological Deep-Inelastic Transfer model (DIT) and, alternatively, with the microscopic Constrained Molecular Dynamics model (CoMD). The de-excitation of the hot heavy projectile fragments was performed with the Statistical Multifragmentation Model (SMM). An overall good description of the available data was obtained with the models employed. Furthermore, we performed calculations with a radioactive beam of ^{92}Kr (15 MeV/nucleon) interacting with a target of ^{238}U . We observed that the multinucleon transfer mechanism leads to extremely neutron-rich nuclides toward and beyond the astrophysical r-process path.

1 Introduction

The exploration of the nuclear landscape toward the astrophysical r-process path and the neutron drip-line are at the center of interest of the nuclear physics community [1]. Essential to this development is the efficient production of neutron-rich nuclides which constitutes a central issue in current and upcoming rare isotope beam facilities worldwide (see, e.g., [2,3,4,5,6,7,8,9,10,11]).

The traditional routes to produce neutron-rich nuclides are spallation, fission and projectile fragmentation [12]. Spallation is an efficient mechanism to produce rare isotopes for ISOL-type techniques [13]. Projectile fission is appropriate in the region of asymmetric fission peaks of the light and heavy fission fragments (see, e.g., [14]). Finally, projectile fragmentation constitutes a general approach to produce exotic nuclei at beam energies above 100 MeV/nucleon (see, e.g., [15,16]). This approach is, nevertheless, limited by the fact that optimum neutron excess in the fragments is achieved by stripping the maximum possible number of protons (and a minimum possible number of neutrons). Surpassing the limits of the traditional approaches and reaching out to the neutron dripline is highly desirable at present. Thus, the study of new synthesis routes constitutes a vigorous endeavor of the nuclear science community.

Toward this end, to reach a high neutron-excess in the products, apart from proton stripping, it is necessary to pickup neutrons from the target. Such a possibility is offered by reactions of nucleon exchange at beam energies from the Coulomb barrier [17,18] to the Fermi energy (20–40 MeV/nucleon) [19,20]. Detailed experimental data in this broad energy range are limited at present [18,21,22]. In multinucleon transfer and deep-inelastic reactions near the Coulomb barrier [18], the low velocities of the fragments and the wide angular and ionic charge state distributions may limit the collection efficiency for the most neutron-rich products. However, the reactions in the Fermi energy regime (15–35 MeV/nucleon) combine the advantages of both low-energy (i.e., near and above the Coulomb barrier) and high-energy (i.e., above 100 MeV/nucleon) reactions. At this energy, the interaction of the projectile with a neutron-rich target enhances the N/Z of the fragments, while the velocities remain high enough to allow efficient in-flight collection and separation.

Our initial experimental studies of projectile fragments from 25 MeV/nucleon reactions of ^{86}Kr on ^{64}Ni [19] and ^{124}Sn [20] indicated substantial production of neutron-rich fragments. Motivated by developments in several facilities that will offer either very intense primary beams [4,7,9] at this energy range or re-accelerated rare isotope beams [3,4,7,8,9], we continued our experimental and theoretical studies at 15 MeV/nucleon [23,29,30,31].

In this contribution, we present our study of the production cross sections and

the angular distributions of projectile fragments from collisions of a ^{86}Kr (15 MeV/nucleon) beam with heavy targets. Data from our experimental work at Texas A&M are compared with calculations based on either the phenomenological deep-inelastic transfer (DIT) model, or the microscopic constrained molecular dynamics model (CoMD). A overall good description of the experimental data with DIT or CoMD was obtained, suggesting the possibility of using the present theoretical models to predict the production of exotic nuclei employing radioactive beams. As an example, we will show production cross sections and rates of neutron-rich isotopes from a radioactive beam of ^{92}Kr (15 MeV/nucleon) interacting with a ^{238}U target.

2 Outline of Results and Comparisons

A detailed presentation of our previously obtained experimental data appear in [23] in which the mass spectrometric measurements of production cross sections of neutron-rich projectile fragments from the reactions of a 15 MeV/nucleon ^{86}Kr beam with $^{64,58}\text{Ni}$ and $^{124,112}\text{Sn}$ targets were presented. We also mention that the experimental data of 25 MeV/nucleon ^{86}Kr -induced reactions are described in detail in our articles [19,20,21,22].

2.1 Study of Production Cross Sections

In Fig. 1, we present the experimental mass distributions of projectile-like fragments with $Z = 37-30$ from the reaction ^{86}Kr (15 MeV/nucleon) + ^{124}Sn [23] and compare them with the calculations using the DIT code [24,25] (solid yellow line) and the CoMD code [27,28] (solid red line). Both dynamical codes were combined with the Statistical Multifragmentation Model (SMM) [26] used for the de-excitation of the hot quasi-projectiles emerging after the dynamical stage of the reaction. The results of the calculations are in overall good agreement with the experimental data especially for isotopes close to the projectile with $Z = 36-32$. We note that in some of the Kr isotopes ($A=86,89,90$), the experimental cross sections are especially high because of contamination from elastically scattered beam. The overestimation of the cross sections for n-rich products with $Z=31$ and 30 from the CoMD calculation may be related to issues of low excitation energy, as currently calculated in CoMD [29].

Furthermore, in Fig. 2 we show the DIT/SMM calculations of projectile-like fragments from the reaction ^{86}Kr (15 MeV/nucleon) + ^{238}U (solid yellow line). We have chosen the heaviest and most neutron-rich target available in order to explore how far in N/Z we can go with this reaction. Also, we chose to study the reaction with the ^{238}U target, but with a radioactive beam of ^{92}Kr (15

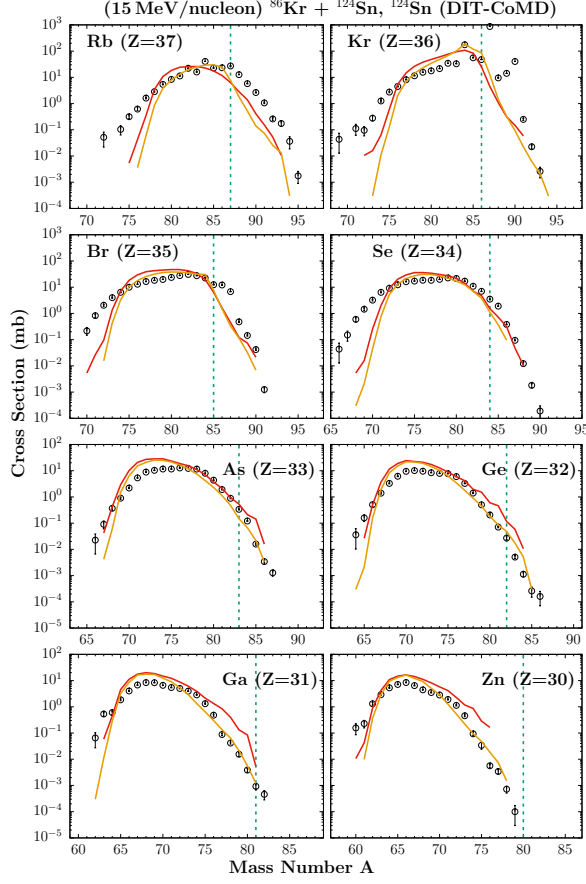


Fig. 1. Experimental mass distributions (open black circles) of elements with $Z = 37-30$ from the reaction $^{86}\text{Kr}(15 \text{ MeV/nucleon}) + ^{124}\text{Sn}$ [23] compared with DIT/SMM calculations (yellow line) and CoMD/SMM calculations (red line).

MeV/nucleon) (dashed yellow line). As there are no experimental data with the ^{238}U target, we used the data from $^{86}\text{Kr}(15 \text{ MeV/nucleon}) + ^{124}\text{Sn}$ for reference. We observe that the distributions extend far to the neutron-rich side especially when the radioactive beam is used. This tendency is pronounced for isotopes rather close to the projectile ($Z=34-36$).

We point out that, for, e.g., bromine ($Z=35$), isotopes that have up to 15 more neutrons ($A = 96$) than the corresponding stable isotope ($A = 81$) can be obtained. Thus, by using neutron-rich radioactive beams, and via the mechanism of peripheral multinucleon transfer, we have the possibility to produce extremely neutron-rich nuclides. We note that similar observations were made for the reaction with lighter projectiles (of Ar and Ca) on the ^{238}U target in our recent article [31]. We do not have experimental data for the $^{86}\text{Kr} + ^{238}\text{U}$ reaction, but we have plans to study it in the near future.

A comprehensive presentation of the DIT/SMM calculated production cross sections of the projectile fragments from the above reaction on the Z vs N plane is given in Fig. 3. In this figure, stable isotopes are represented by closed

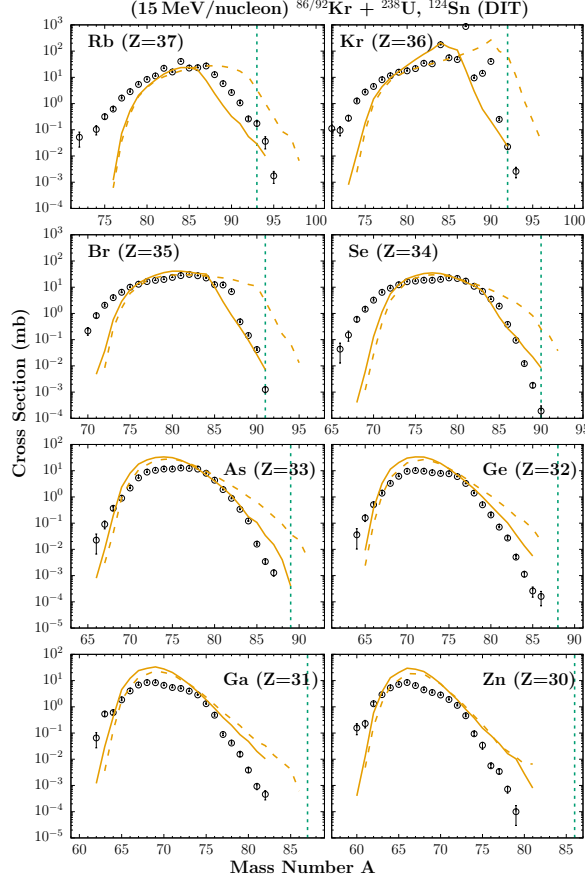


Fig. 2. DIT/SMM calculated mass distributions of elements with $Z = 37-30$ from the reaction of a radioactive beam of ^{92}Kr (15 MeV/nucleon) interacting with a ^{238}U target (dashed yellow line), compared to the DIT/SMM calculations of the stable beam reaction $^{86}\text{Kr} + ^{238}\text{U}$ (solid yellow line). The experimental mass distributions (open points) from ^{86}Kr (15 MeV/nucleon) + ^{124}Sn [23] are also given for reference.

squares, whereas fragments obtained by the $^{92}\text{Kr} + ^{238}\text{U}$ reaction are given by the open circles, with sizes corresponding to cross-section ranges according to the figure key. The green line gives the location of the neutron drip-line and the purple line indicates the expected path of the astrophysical rapid neutron-capture process (r-process). Using this representation of the previous calculation, we clearly observe that the neutron pickup products from ^{92}Kr reach and even exceed the path of the r-process near $Z=30-36$.

In Table I, we summarize the calculated cross sections and production rates of several neutron-rich isotopes from the reaction of the radioactive beam of ^{92}Kr (15 MeV/nucleon) with the ^{238}U target. For the rate calculations, the ^{92}Kr beam with intensity of 1.0 pA (6.2×10^9 particles/sec) is assumed to interact with a ^{238}U target of 20 mg/cm² thickness. We see that it is possible to produce extremely neutron-rich isotopes in these reactions with the use of re-accelerated radioactive beams, such as ^{92}Kr , that will become available in upcoming rare-isotope facilities (e.g. [9,10,11]). Along these lines, we wish

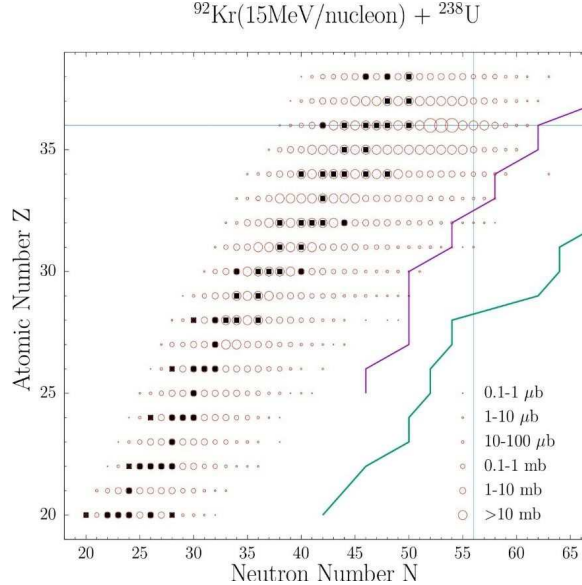


Fig. 3. Representation of DIT/SMM calculated production cross sections of projectile fragments from the radioactive-beam reaction ^{92}Kr (15 MeV/nucleon) + ^{238}U on the Z–N plane. Cross section ranges are shown by open circles according to the key. Closed squares show the stable isotopes. The purple line shows the astrophysical r-process path and the green line shows the neutron drip-line. The horizontal and vertical lines indicate, respectively, the Z and N of the ^{92}Kr projectile.

to continue this work at the following facilities: a) the Cyclotron Institute of Texas A&M University using the MARS separator, b) the LNS/Catania using beams from the S800 Cyclotron and employing the MAGNEX spectrometer, and c) the RISP facility with stable and radioactive beams from the RAON accelerator complex using the KOBRA separator.

2.2 Study of Angular Distributions

After the description of the production cross sections, which have been the main focus of our work so far, we initiated a detailed study of the angular distributions of the projectile-like fragments. In regards to experimental data, we refer again to our previous work [23] with the MARS spectrometer. As described in [23], the data were obtained at two angle settings, by sending the beam on the target at the appropriate angle in the MARS target chamber. The angle settings were: the 4.0° setting and the 7.5° setting, covering the polar angular ranges of $\Delta\theta=2.2^\circ-5.8^\circ$, and $\Delta\theta=5.6^\circ-9.2^\circ$, respectively. We remind that appropriate integration of these data provided the total production cross sections that are reported in [23] and presented in Figs. 1,2.

We start our presentation with the angular distributions of selected projectile fragments from the reaction of $^{86}\text{Kr}+^{124}\text{Sn}$ at 15 MeV/nucleon (Figures 4,5

Table 1

Cross sections and rate estimates (last column) of very neutron-rich isotopes from the reaction ^{92}Kr (15 MeV/nucleon) + ^{238}U . For the rates, a radioactive beam of ^{92}Kr with intensity 1.0 particle nA (6.2×10^9 particles/s) is assumed to interact with a ^{238}U target of 20 mg/cm² thickness.

Rare Isotope	Reaction Channel	Cross Section (mb)	Rate (sec ⁻¹)
^{93}Kr	-0p+1n	12	3.6×10^3
^{94}Kr	-0p+2n	1.3	3.9×10^2
^{95}Kr	-0p+3n	0.3	90
^{96}Kr	-0p+4n	0.05	15
^{92}Br	-1p+1n	0.8	2.4×10^2
^{93}Br	-1p+2n	0.2	60
^{94}Br	-1p+3n	0.07	21
^{95}Br	-1p+4n	0.02	6
^{96}Br	-1p+5n	0.008	2
^{90}Se	-2p+0n	0.25	75
^{91}Se	-2p+1n	0.14	42
^{92}Se	-2p+2n	0.05	15
^{93}Se	-2p+3n	0.02	6

and 6). For this system, the grazing angle is $\theta_{gr} \simeq 9.0^\circ$. (A vertical dashed line indicates this angle in the figures.) We, thus, expect that the 7.5° angle setting is the appropriate one to efficiently collect the quasi-elastic products, as has been discussed in [23,29].

The experimental data of the differential cross sections for each nuclide consist of two points: one at $\theta=4.0^\circ$ and the other at $\theta=7.5^\circ$, each plotted with horizontal error bars indicating the polar angular acceptance of $\Delta\theta = 3.6^\circ$. (The vertical error bars indicate, as usual, the statistical uncertainties). The data are compared with calculations employing the DIT model (yellow symbols) and the CoMD model, both followed by the SMM model, as also shown in the previous comparisons for the cross sections. The calculations were binned and presented in angular steps of two degrees.

Three different of calculations were performed with the CoMD model. a) The "standard" calculation (red symbols) using standard parameters of the CoMD

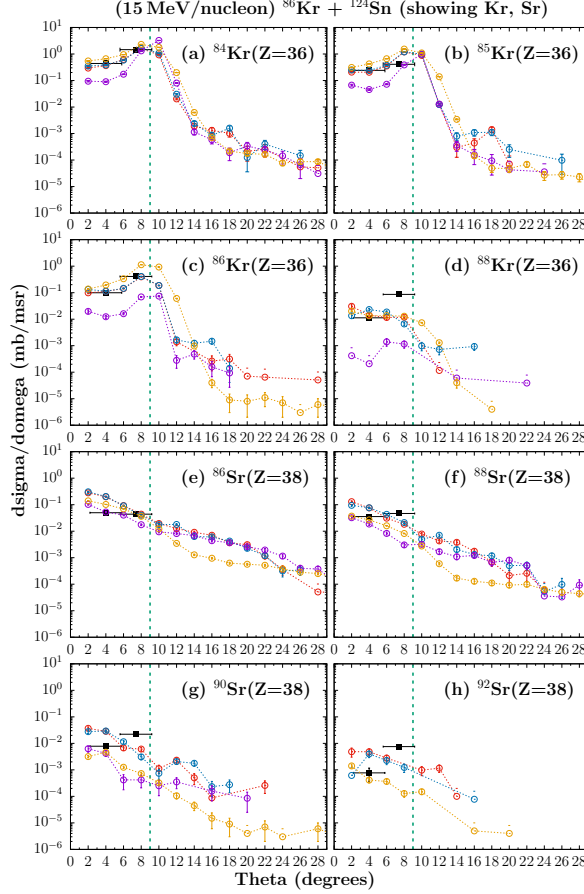


Fig. 4. Angular distributions of neutron rich isotopes of $_{36}\text{Kr}$ and $_{38}\text{Sr}$ from the reaction of ^{86}Kr (15 MeV/nucleon) with ^{124}Sn . Black squares (with horizontal error bars): experimental data [23]. Symbols connected with dotted lines: calculations as follows. Yellow symbols: DIT. Red symbols: standard CoMD. Blue symbols: CoMD with pairing. Purple symbols: CoMD with compressibility $K=272$ MeV.

code, as in our previous works [29,31]. b) A calculation with pairing (blue symbols). For this calculation, we introduced a phenomenological description of n-n and p-p pairing, according to the recent article [32]. In this description, for two neutrons (or protons) that have anti-parallel spins and energies near the Fermi energy, an additional attractive interaction was introduced with strength adjusted to reproduce the empirical pairing energy of the Bethe-Weizsacker equation. c) a calculation in which the compressibility of cold symmetric nuclear matter was increased to $K=272$ MeV (purple symbols). We remind that in the "standard" CoMD calculation, the parameters of the effective interaction correspond to a compressibility of $K=200$ MeV.

In the upper half of Fig. 4, we show the angular distributions for Krypton ($Z=36$). For $A=86$, we see that the data point at $\theta=7.5^\circ$ is higher than that at $\theta=4.0^\circ$, as expected. This step seems to be described by the DIT calculation, despite the larger value of the latter at $\theta=8^\circ$ and $\theta=10^\circ$. The CoMD calculations (in all three variations) appear to describe the shape of the angular

distribution rather well; the CoMD calculation with $K=272$ is however lower than the other calculations. For $A=85$ and $A=84$, there is some agreement of the calculations with the data. However, for $A=88$ (+2n channel) the calculations cannot describe the step in the data. This may be related to enhanced neutron-pair transfer, possibly beyond our tentative pairing calculation.

In the lower half of Fig. 4, we show the angular distributions for Strontium ($Z=38$, +2p channels). For $A=88$, we note that the +2p channel does not peak at the grazing angle as the +2n channel (Fig. 8d). Moreover, for $A=86$, the removal of neutrons leads to a flat distribution in the data. The addition of neutrons, however, leads to angular distributions peaked at θ_{gr} . This feature cannot be described by DIT or CoMD, and requires further investigation.

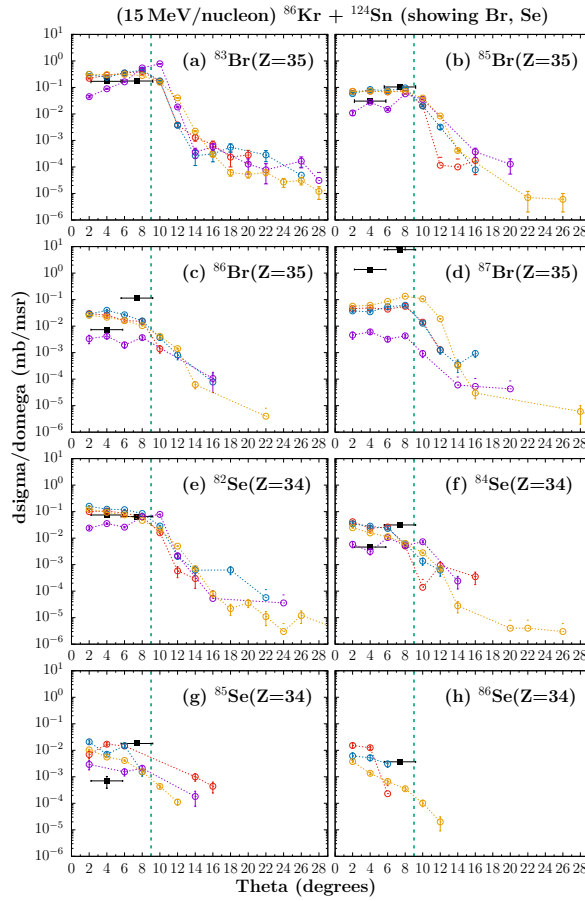


Fig. 5. Angular distributions of neutron rich isotopes of $_{35}\text{Br}$ and $_{34}\text{Se}$ from the reaction of ^{86}Kr (15 MeV/nucleon) with ^{124}Sn . Black squares (with horizontal error bars): experimental data [23]. Symbols connected with dotted lines: calculations as follows. Yellow symbols: DIT. Red symbols: standard CoMD. Blue symbols: CoMD with pairing. Purple symbols: CoMD with compressibility $K=272$ MeV.

In the upper half of Fig. 5, we show the angular distributions of several isotopes of bromine ($Z=35$). For $A=85$ (-1p channel), the calculations describe

rather well the $\theta=7.5^\circ$ data point, but are higher than the $\theta=4.0^\circ$ data point. Interestingly, the CoMD calculation with $K=272$ MeV appears to describe both data points well. Again, the removal of neutrons ($A=83, -1p-2n$) results in a nearly flat angular distribution that seems to be described by the calculations. Concerning the neutron pickup nuclides ($A=86, -1p+1n$) and ($A=87, -1p+2n$), the experimental data are peaked at θ_{gr} and cannot be described by the DIT and CoMD calculations. We think that for $A=87$ ($-1p+2n$), the experimental data may be contaminated from background of elastically scattered beam. Moreover, especially for $A=86$, we speculate that part of the discrepancy may be due to a contribution of a single charge exchange (SCE) process that, of course, cannot be described by DIT or CoMD.

In the lower half of Fig. 5, we show the angular distributions of several isotopes of Selenium ($Z=34$) ($-2p$ channels). Observations similar to those of the previous figure pertain here. For $A=82$ ($-2p-2n$), the experimental angular distribution is rather flat and is well described by the calculations. However, for $A=84$ ($-2p$), the experimental angular distribution is again peaked at θ_{gr} and cannot be adequately described by the calculations. The situation for the angular distributions of $A=85$ ($-2p+1n$) and $A=86$ ($-2p+2n$) is similar to the previous ones. We may attribute the discrepancy for $A=85$ in part to a contributing SCE process along with a $+1n$ process. For $A=86$ ($-2p+2n$), we speculate that, a DCE (double charge exchange) process might also contribute, along with two successive SCE processes. The subject of potential contributions of SCE and DCE processes in these heavy-ion reactions below the Fermi energy is currently under investigation by our group via systematic studies of the momentum distributions of the relevant nuclides, and may shed light to interesting aspects of the reaction mechanism(s).

In Fig. 6, we show the angular distributions for several isotopes of Arsenic ($Z=33, -3p$ channels) in the upper half, and Germanium ($Z=32, -4p$ channels) in the lower half. The angular distributions of these nuclides reveal features analogous to those of the nuclides shown in the previous figures. Specifically, the "cold" proton removal channels ($-3p$ and $-4p$, respectively) are peaked at θ_{gr} (only one point in the data), whereas the DIT and CoMD calculations show, as before, a monotonic decrease with increasing angle. Furthermore, we notice a transition from a θ_{gr} peaked angular distribution to a flat distribution between $A=82$ to $A=80$ for As, and, between $A=80$ to $A=78$ for Ge.

We now present the angular distributions of selected projectile fragments from the reaction of ^{86}Kr (15 MeV/nucleon) + ^{64}Ni in Figs. 7 and 8. For this system, the grazing angle is $\theta_{gr} \simeq 6.0^\circ$. (A vertical dashed line indicates this angle in Figs. 7 and 8). We expect that the 4.0° angular setting is the optimum for the efficient collection of quasi-elastic products [23]. The general feature of the experimental angular distributions is that the 4.0° data points are higher than the corresponding 7.5° ones. In the upper half of Fig. 7, we show the angular

distributions of several isotopes of Krypton ($Z=36$). For $A=86$, the data point at $\theta=4.0^\circ$ is, as expected, higher than that at $\theta=7.5^\circ$. This step seems to be described by the calculations, which are however lower than the data. For $A=85$ and $A=84$, there is a better agreement of the calculations with the data. However, again in the two-neutron pickup channel, $A=88$, the calculations are substantially lower than the experimental data. In the lower part of Fig. 7, we present the angular distributions of several isotopes of Strontium ($Z=38$, +2p channels). For these isotopes, the calculations appear to describe the decreasing trend of the data with increasing angle.

In the upper part of Fig. 8, we show the angular distributions of several isotopes of Bromine ($Z=35$, -1p channels). For $A=85$ (-1p), there is a satisfactory description of the data by the calculations. This is also true for the neutron removal channel, $A=83$ (-1p-2n). As we move to the neutron pickup channels, $A=86$ (-1p+1n), and $A=87$ (-1p+2n), the calculations appear to be substan-

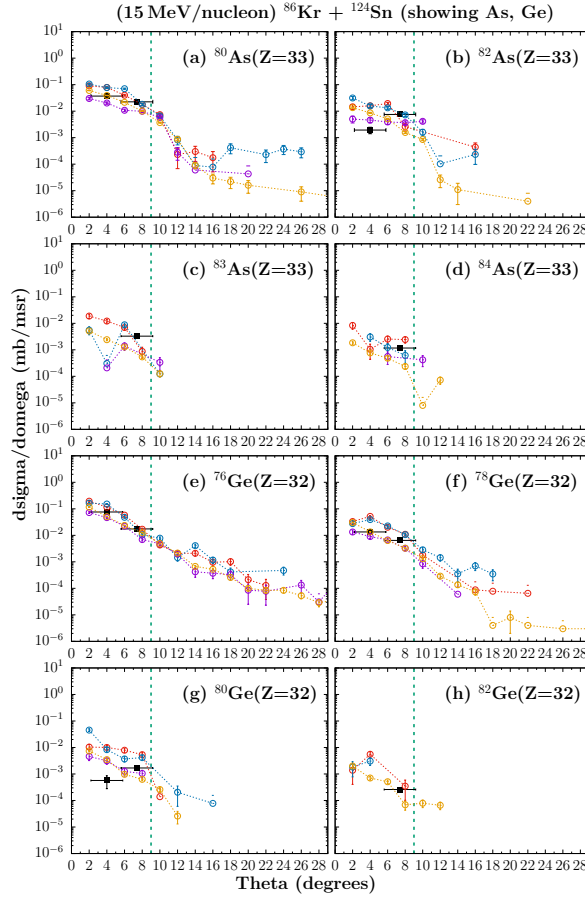


Fig. 6. Angular distributions of neutron rich isotopes of ${}_{33}\text{As}$ and ${}_{32}\text{Ge}$ from the reaction of ${}^{86}\text{Kr}$ (15 MeV/nucleon) with ${}^{124}\text{Sn}$. Black squares (with horizontal error bars): experimental data [23]. Symbols connected with dotted lines: calculations as follows. Yellow symbols: DIT. Red symbols: standard CoMD. Blue symbols: CoMD with pairing. Purple symbols: CoMD with compressibility $K=272$ MeV.

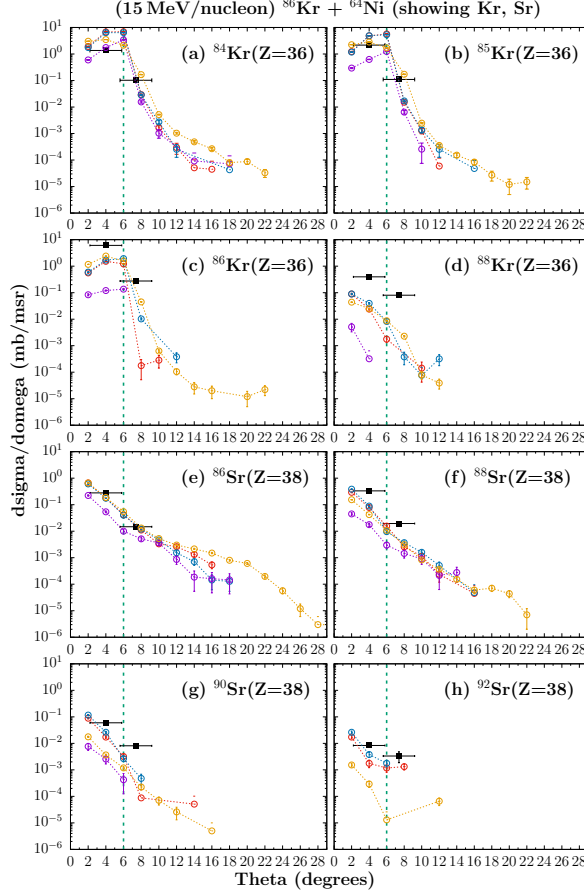


Fig. 7. Angular distributions of neutron rich isotopes of $_{36}\text{Kr}$ and $_{38}\text{Sr}$ from the reaction of ^{86}Kr (15 MeV/nucleon) with ^{64}Ni . Black squares (with horizontal error bars): experimental data [23]. Symbols connected with dotted lines: calculations as follows. Yellow symbols: DIT. Red symbols: standard CoMD. Blue symbols: CoMD with pairing. Purple symbols: CoMD with compressibility $K=272$ MeV.

tially lower than the experimental data. In the lower part of Fig. 8, we show the angular distributions of several nuclides of Selenium ($Z=34$, $-2p$ channels). Observations similar to those of the upper half of figure pertain here. Specifically, for $A=84$ ($-2p$) the calculations appear to follow the data to some extent. Moving to the neutron removal channel, for $A=82$ ($-2p-2n$) the calculations describe the data fairly well. Finally, for the neutron pickup channels, $A=85$ ($-2p+1n$), and $A=86$ ($-2p+2n$) the calculations again follow the trend of the data, but are lower than them.

As a general remark of the angular distribution study, we point out that a rather satisfactory overall agreement of the calculations with the experimental data was achieved. Several discrepancies were noticed and are the subject of further investigation. As expected, the angular distributions of the $\text{Kr}+\text{Sn}$ system are more extended than the $\text{Kr}+\text{Ni}$ system, which are more forward focused due to inverse kinematics.

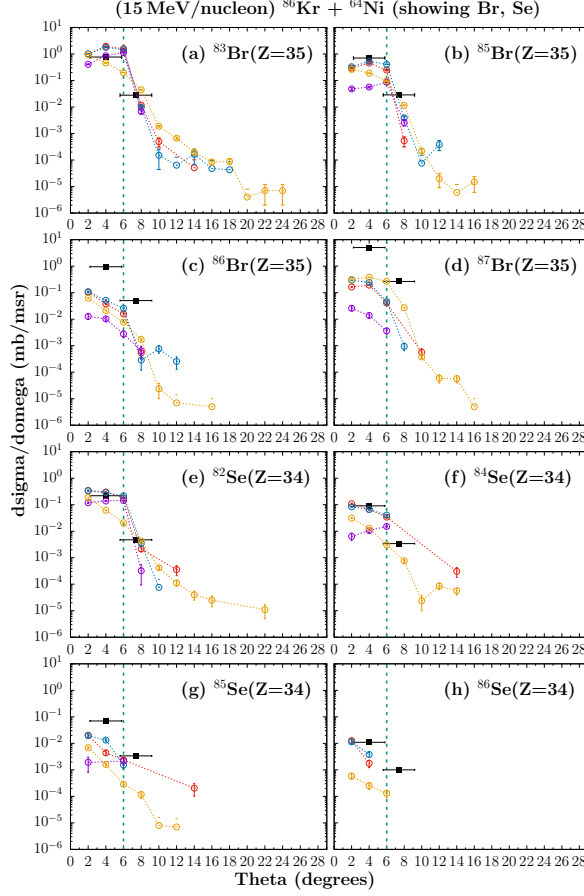


Fig. 8. Angular distributions of neutron rich isotopes of $_{35}\text{Br}$ and $_{34}\text{Se}$ from the reaction of ^{86}Kr (15 MeV/nucleon) with ^{64}Ni . Black squares (with horizontal error bars): experimental data [23]. Symbols connected with dotted lines: calculations as follows. Yellow symbols: DIT. Red symbols: standard CoMD. Blue symbols: CoMD with pairing. Purple symbols: CoMD with compressibility $K=272$ MeV.

Referring to the Kr+Sn system, the DIT calculations are rather similar in most cases to the CoMD calculations, especially to the standard CoMD calculation and the CoMD calculation with the pairing. Specifically, the CoMD calculation with the pairing seems to be slightly higher than the standard CoMD calculation for large angles (where, of course, there are no experimental data). Finally, the effect of the compressibility in the CoMD code was investigated by performing calculations with $K=272$ MeV, along with the standard value of $K=200$ MeV in the other CoMD calculations. We observed that with $K=272$, the CoMD calculated angular distributions are peaked more toward the θ_{gr} , as compared to those with the "standard" value of $K=200$ MeV, and are thus in better agreement with the data. However, they have the tendency to be lower than the other CoMD calculations.

3 Summary and Conclusions

In this contribution, we presented our recent studies of production cross sections and angular distributions of projectile fragments from ^{86}Kr -induced reactions at 15 MeV/nucleon. We studied the cross sections and the angular distributions of neutron-rich nuclides from collisions of a ^{86}Kr (15 MeV/nucleon) beam with several heavy targets (^{64}Ni , ^{124}Sn and ^{238}U). Experimental data from our previous work at Texas A&M were compared with model calculations. The calculations were based on a two-step approach: the dynamical stage of the collision was described with either the Deep-Inelastic Transfer model (DIT), or with the microscopic Constrained Molecular Dynamics model (CoMD). The de-excitation of the hot heavy projectile fragments was performed with the Statistical Multifragmentation Model (SMM). We first studied the production cross sections of neutron-rich nuclides from collisions of a ^{86}Kr (15 MeV/nucleon) beam with ^{124}Sn and ^{238}U . We also proceeded with calculations with a radioactive beam of ^{92}Kr (15 MeV/nucleon) with ^{238}U and observed that the multinucleon transfer mechanism leads to very neutron-rich nuclides in the mass region $A=80-100$ toward and beyond the r-process path.

Subsequently, we initiated a study of the angular distributions of projectile fragments from the reactions of ^{86}Kr (15 MeV/nucleon) with targets of ^{64}Ni and ^{124}Sn . We compared our experimental data at the two angle settings of the MARS spectrometer, namely at 4.0° and at 7.5° , with detailed calculations using the DIT and CoMD models. Three variants of the CoMD calculations were performed: the standard calculation (as in all our previous works), b) a calculation including a pairing interaction, and c) a calculation with compressibility $K=272$ for symmetric nuclear matter. A rather satisfactory agreement of the calculations with the experimental data was obtained. Several discrepancies were noticed and are the subject of further investigation.

Our current studies indicate that heavy-ion reactions below the Fermi energy can be exploited as an effective route to access extremely neutron-rich isotopes toward the r-process path and the neutron drip-line. In this vein, future experiments in several accelerator facilities may be planned that will enable a variety of nuclear studies in unexplored regions of the nuclear chart.

References

- [1] J. Erler et al, *Nature* **486**, 509 (2011).
- [2] D. F. Geesaman, C. K. Gelbke, R. V. F. Janssens, B. M. Sherrill, *Ann. Rev. Nucl. Part. Sci.* **56**, 53 (2006)
- [3] FRIB main page: www.frib.msu.edu

- [4] GANIL main page: www.ganil.fr
- [5] GSI main page: www.gsi.de
- [6] RIBF main page: www.rarf.riken.go.jp/Eng/facilities/RIBF.html
- [7] ATLAS main page: www.phy.anl.gov/atlas/facility/index.html
- [8] EURISOL main page: www.eurisol.org
- [9] RISP main page: www.risp.re.kr/eng/pMainPage.do
- [10] K. Tshoo, Y. K. Kim, Y. K. Kwon et al, Nucl. Instrum. Methods B **317**, 242 (2013).
- [11] K. Tshoo, H. Chae, J. Park, J.Y. Moon, Y.K. Kwon, G.A. Souliotis et al, Nucl. Instrum. Methods B **376**, 188 (2016).
- [12] Y. Blumenfeld, T. Nilsson and P. Van Duppen, Phys. Scr. T152 014023 (2013).
- [13] A. Kelić, M. V. Ricciardi, K. -H. Schmidt, BgNS Transactions, **13**, 98 (2009).
- [14] H. Alvarez-Pol et al., Phys. Rev. C **82**, 041602 (2010).
- [15] O. B. Tarasov et al., Phys. Rev. C **80**, 034609 (2009).
- [16] S. Lukyanov et al., Phys. Rev. C **80**, 014609 (2009).
- [17] V. V. Volkov, Phys. Rep. **44**, 93 (1978).
- [18] L. Corradi, G. Pollarolo, S. Szilner, J. Phys. G **36**, 113101 (2009).
- [19] G. A. Souliotis et al., Phys. Lett. B **543**, 163 (2002).
- [20] G. A. Souliotis et al., Phys. Rev. Lett. **91**, 022701 (2003).
- [21] G. A. Souliotis et al., Nucl. Instrum. Methods **B 204** 166 (2003).
- [22] G. A. Souliotis et al., Nucl. Instrum. Methods **B 266**, 4692 (2008).
- [23] G. A. Souliotis et al., Phys. Rev. C **84**, 064607 (2011).
- [24] L. Tassan-Got and C. Stephan, Nucl. Phys. **A 524**, 121 (1991).
- [25] M. Veselsky and G.A. Souliotis, Nucl. Phys. **A 765**, 252 (2006).
- [26] J. Bondorf et al., Phys. Rep. **257**, 133 (1995).
- [27] M. Papa et al., Phys. Rev. **C 64**, 024612 (2001).
- [28] M. Papa et al, J. Comp. Phys. **208**, 403 (2005).
- [29] P.N. Fountas, G.A. Souliotis, M. Veselsky and A. Bonasera, Phys. Rev. C **90**, 064613 (2014).
- [30] N. Vonta, G.A. Souliotis et al., Phys. Rev. C **92**, 064611 (2016).
- [31] A. Papageorgiou, G.A. Souliotis et al., Journal of Physics G **45**, 095105 (2018).
- [32] C. Agodi, G. Giuliani, F. Cappuzzello, A. Bonasera, et al., Physical Review C **97**, 034616 (2018).